







Exponential dependence of interlayer exchange coupling in Fe/MgO(001) superlattices on temperature

Nanny Strandqvist ¹, Tobias Warnatz ¹, Kristbjörg Anna Thórarinsdóttir ², Alexei Vorobiev ^{1,3},
Vassilios Kapaklis ¹ and Björgvin Hjörvarsson ¹

¹*Department of Physics and Astronomy, Uppsala University, Box 516, SE-75120 Uppsala, Sweden*

²*Science Institute, University of Iceland, Dunhaga 3, IS-107 Reykjavik, Iceland*

³*Institute Laue-Langevin, 71 avenue des Martyrs, 38042 Grenoble, France*



(Received 9 May 2025; accepted 8 January 2026; published 9 February 2026)

The interlayer exchange coupling in Fe/MgO(001) superlattices is found to increase exponentially with decreasing temperature. Around 150 K, the field-induced response changes from discrete switching—governed by field-driven domain propagation—to a collective rotation of the magnetic layers. This transition is accompanied by a change in the magnetic ground state from 180° (antiferromagnetic) to 90° alignment between adjacent Fe layers. These effects are argued to arise from quantum-well states, defined by the total thickness of the samples.

DOI: [10.1103/r9vz-kqvm](https://doi.org/10.1103/r9vz-kqvm)

I. INTRODUCTION

Artificial superlattices are fascinating materials that provide a versatile platform for exploring emergent physical phenomena. Furthermore, their properties can be tailored by, e.g., the choice of constituents, the thickness, and the thickness ratio of the layers [1–4]. In semiconductor superlattices, the proximity of layers with different band gaps leads to the formation of quantum-well states, with their own electronic structure and properties [5]. Similar quantum effects are observed in metallic superlattices where magnetic layers couple across nonmagnetic layers through oscillatory interlayer exchange coupling (IEC) [6]. In layers, such as MgO, the coupling strength is known to decrease exponentially with increasing thickness of the layer, which is typically attributed to spin-polarized tunneling [7–10].

Almost all prior studies on IEC in Fe/MgO heterostructures are based on trilayers, with a primary focus on device-related functionalities [11–15]. It is only recently the investigation of interlayer exchange coupling has been extended to include Fe/MgO(001) superlattices [10,16–18]. These can exhibit discontinuous steps in the field response (digital hysteresis), arising from switching of individual Fe layers—a behavior attributed to the interplay between antiferromagnetic IEC and the intrinsic magnetic anisotropy of the Fe layers [10]. Moreover, the magnetic response has been found to depend on the number of Fe/MgO repetitions, which was argued to arise from long-range magnetic IEC [16,17]. The thickness of the Fe layers has also a profound effect on the strength of the IEC [18]. These findings highlight the need to account for all

length scales in the structure—including the MgO spacer, Fe layer, and the total thickness of the stack—when describing the coupling. Here, we will explore the underlying principles behind the IEC in Fe/MgO(001) superlattices. We do this by exploring the temperature dependence of the coupling in structures with different number of repeats of the Fe/MgO layers.

II. RESULTS

The growth and the structural characterization of the superlattices are briefly described in the Supplemental Material [19] and cited references. The magnetic response was investigated using the magneto-optical Kerr effect (MOKE) and vibrating sample magnetometer (VSM). Normalized room-temperature hysteresis loops for [Fe(2 nm)/MgO(1.7 nm)]_N (001) superlattices with $N = 2, 4, 8,$ and 10 bilayer repetitions are shown in Fig. 1. These measurements were conducted with an external magnetic field applied along an Fe [001] easy axis and the hysteresis loops were adjusted by the removal of the coercivity of the Fe layers, as described in Ref. [17], to better emphasize the reversibility—or lack thereof—in the switching behavior of the Fe layers. All samples exhibit discrete magnetic switching, characterized by steplike features in the magnetization curves. These steps arise from the nucleation and propagation of 90° domain walls across the full lateral extent of the 2 nm-thick Fe layers across the sample area of 1 cm² [16,20,21]. The switching is driven by the applied magnetic field, while IEC and magnetocrystalline anisotropy act as restoring forces. Consequently, the field value at each step is proportional to the strength of the IEC acting on the switching layer, when the field is aligned with the easy axis. It is worth noting that the coupling is dominated by IEC as contributions from dipolar fields to the coupling can be neglected for the continuous layers [22–25].

For $N = 2$ [see Fig. 1(a)], a magnetic field of approximately 2.4 mT is required to align the magnetic moments

Published by the American Physical Society under the terms of the Creative Commons Attribution 4.0 International license. Further distribution of this work must maintain attribution to the author(s) and the published article's title, journal citation, and DOI. Funded by Bibsam.

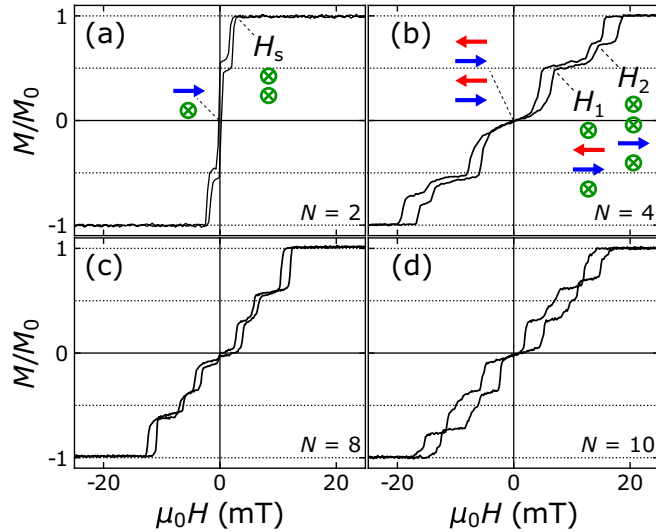


FIG. 1. In-plane hysteresis measured at room temperature by MOKE, along the Fe[100] easy axis for $[\text{Fe}(2.0 \text{ nm})/\text{MgO}(1.7 \text{ nm})]_N(001)$ superlattices with (a) $N = 2$, (b) $N = 4$, (c) $N = 8$, and (d) $N = 10$ bilayer repetitions. The labels H_1 , H_2 , and H_s denote the switching fields associated with each magnetization step, where H_s corresponds to the field required to align all Fe layers.

of both Fe layers (H_s). Upon reducing the field from saturation to zero, a single switching event is observed, resulting in a remanent magnetization of $M/M_0 \approx 0.5$. This value is consistent with the reversal of a single Fe layer, leading to a 90° alignment of the layers. The configuration is likely to be metastable, arising from the competition between a weak antiferromagnetic interlayer exchange coupling and the significantly stronger fourfold magnetocrystalline anisotropy [10,16,22,26].

Increasing the number of bilayers to four ($N = 4$) has a pronounced effect on the hysteresis curve, as shown in Fig. 1(b). In particular, the remanence at zero field becomes negligible, consistent with an antiferromagnetic alignment of the Fe layers. Three discrete steps are observed between remanence and saturation. The first step, occurring at H_1 , is approximately twice as large as the subsequent steps, corresponding to a magnetization change of $M/M_0 \approx 0.5$. This step is attributed to the simultaneous switching of the top and bottom Fe layers, which each have only one nearest neighbor and therefore require a lower switching field—an effect that arises purely from the differing number of magnetic neighbors [16,17]. As the external field increases further, the remaining Fe layers are sequentially switched. The field required to align all four Fe layers parallel to the external field is $H_s \approx 16$ mT. Similar behavior is observed for $N = 8$ and 10 , as shown in Figs. 1(c) and 1(d). The results are consistent with earlier MOKE and neutron studies, demonstrating that the MOKE signal probes the switching throughout the full $[\text{Fe}/\text{MgO}]_N$ multilayer stack [16,17]. A clear change in the relative strength of the coupling is observed. For example, in the sample with $N = 10$, the saturation field is approximately three times larger than H_1 . In the case of nearest-neighbor interactions, H_s would be expected to be twice as large as H_1 (see Fig. S1 in the Supplemental Material [19]). Consequently, rationalization of the

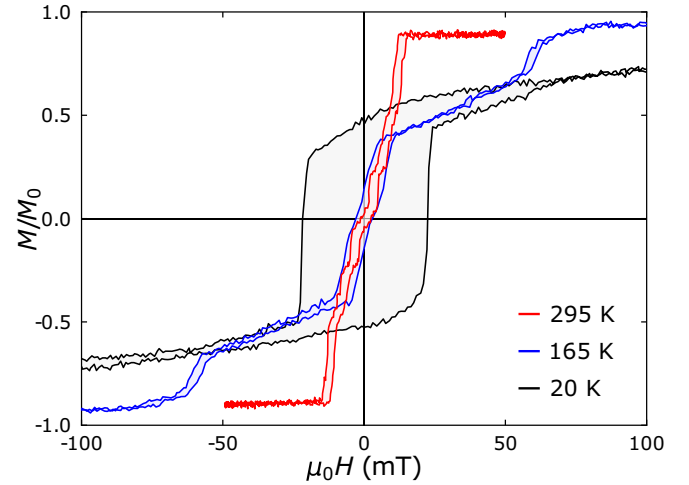


FIG. 2. Normalized hysteresis loops measured along the Fe [100] easy direction for $[\text{Fe}(2 \text{ nm})/\text{MgO}(1.7 \text{ nm})]_{10}$ superlattice at 295, 165, and 20 K (MOKE). The moment of the Fe layers is only modestly affected while the saturation field and the coercivity exhibits much stronger temperature dependence.

switching, within and between samples, requires interactions beyond nearest neighbor [16,17].

Having established the switching properties of the samples at room temperature, we now examine the temperature dependence of the coupling strength in a sample with 10 repeats. For these measurements, the sample was initially cooled to 20 K, and in-plane hysteresis loops were recorded at temperature intervals of 5 K up to 300 K. As seen in Fig. 2, the shape of the hysteresis curve changes markedly with temperature, while the overall Fe moment is only modestly affected. Two discrete switching steps are observed at $T = 165$ K and the magnetization varies linearly between them. In addition, the field required to align the Fe layers parallel to the external field (H_s) increases to approximately 60 mT, indicating a substantial enhancement of the interlayer exchange coupling compared to room temperature. At $T = 20$ K, the (minor-) hysteresis loop is S shaped, bearing little resemblance to the room-temperature response. A large coercivity is observed, and a remanent magnetization of $0.5 M_s$. At this temperature, the discrete steps associated with digital hysteresis have vanished and the field response is consistent with a coherent rotation of the moments in the layers.

To obtain information on the switching of individual layers at different temperatures, we employed polarized-neutron reflectivity (PNR). The PNR measurements were performed on the SuperADAM reflectometer at the Institut Laue-Langevin in Grenoble, France [27]. The neutron wavelength was set to 5.21 Å, with polarization and analyzer efficiencies of 99.8% and 99.9%, respectively, at the incident and receiving ends. The sample was cooled using a liquid-helium cryostat. Data reduction was carried out using the pySArred software package [28], which is used to obtain the corrected neutron flux through normalization to the integrated monitor count. The PNR data were fitted to extract the magnetic profile, with structural parameters (see Supplemental Material [19]) held fixed and only the magnetization angles within the Fe layers

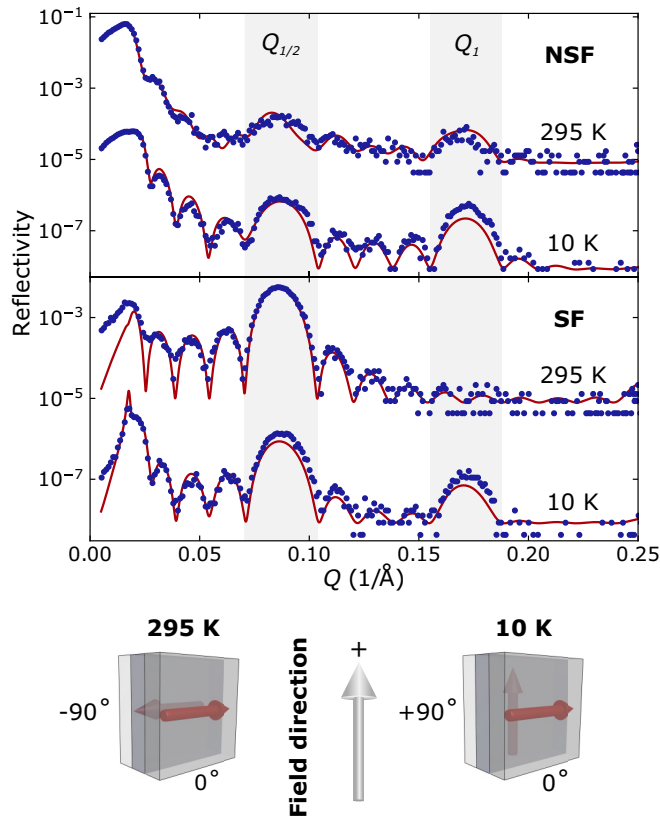


FIG. 3. PNR measurements at 295 and 10 K. Polarized neutron reflectivity data collected in applied fields near remanence (1.5 mT at 295 K and 20 mT at 10 K). The upper panel shows the non-spin-flip (NSF, R^{++}) channel, and the lower panel shows the spin-flip (SF, R^{-+}) channel. Blue dots represent the experimental data, while red curves are the corresponding fits. Shaded gray regions mark the position of the Q_1 and $Q_{1/2}$ peaks.

allowed to change. Structural parameters were obtained by simultaneous fitting of XRR and high-field (500 mT, saturated state, at room temperature) PNR data using the GenX software package [29,30].

Prior to each measurement, a magnetic field of 500 mT was applied in plane along the easy [001] axis, after which the field was reduced to the desired value. The magnetic configuration of the layers was extracted by fitting the non-spin-flip (NSF) reflectivity channels R^{++} and R^{--} , along with the spin-flip (SF) channel R^{-+} . Figure 3 shows the NSF (R^{++}) and SF (R^{-+}) PNR traces at 295 K and 10 K for the sample with $N = 10$. The applied fields were 1.5 mT at 295 K and 20 mT at 10 K. At 295 K, the NSF channel displays a first-order Bragg peak at a scattering vector $Q_1 = \frac{2\pi}{\Lambda} = 0.172 \text{ \AA}^{-1}$, originating from the structural periodicity of the superlattice, where Λ is the Fe/MgO bilayer thickness. In addition, a weak half-order peak $Q_{1/2}$ is observed, with its presence indicating a magnetization component along the applied-field direction with twice the structural periodicity. The SF channel, which is sensitive to transverse magnetic components, shows a well-defined $Q_{1/2}$ peak, indicating alternating transverse components in every second Fe layer. Simultaneous fitting of the PNR and XRR data yields an average angle of 180° between adjacent Fe

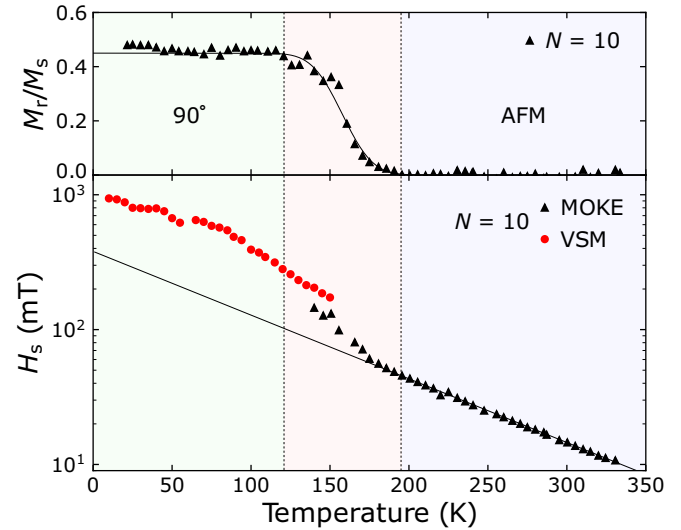


FIG. 4. Temperature dependence of magnetic response. (Top) Remanent magnetization M_r of the $[\text{Fe}/\text{MgO}]_{10}$ superlattice as a function of temperature, normalized to the saturation magnetization M_s . A transition in magnetic ordering is observed around 150 K. (Bottom) Saturation field H_s as a function of temperature. Exponential change in H_s is observed over a broad temperature range. VSM was used for measurement below 165 K.

layers. The layers are therefore antiferromagnetically ordered at room temperature. At 10 K, the PNR data, see Fig. 3, exhibit well-defined Q_1 and $Q_{1/2}$ peaks in both the NSF and SF channels. These features arise from alternating parallel and perpendicular magnetization components in every second Fe layer. Fitting the data reveals that every second layer is aligned along the applied field, while the intervening layers are oriented nearly perpendicular to the applied field, as illustrated in Fig. 3.

Having established the magnetic order within the sample, we can now address the temperature dependency of the magnetic response. The upper panel of Fig. 4 shows the temperature dependence of the ratio of the remanent and saturation magnetization, M_r/M_s , for the sample with $N = 10$. Two distinct temperature regions are observed: between 180 and 330 K, the layers are antiferromagnetically aligned. Below 120 K, the remanence is $M_r/M_s \approx 0.5$, as expected from a $\pi/2$ configuration between adjacent Fe layers. At $T = 300$ K, the saturation field H_s is approximately 14 mT. Upon cooling, H_s increases exponentially, reaching 940 mT at 10 K, as shown in the lower panel of Fig. 4. A distinct change in the temperature dependence of the coupling strength is observed at around 180 K, coinciding with the onset of the reorientation of the moment of the layers, from π to $\pi/2$. Notably, the exponential increase in H_s appears to follow similar temperature dependence, above and below the transition region.

Having established the temperature dependence of the saturation field, we now examine the evolution of the switching field of the outermost layers (H_1) with respect to the saturation of the sample (H_s), which we illustrate in Fig. 5 for the $[\text{Fe}/\text{MgO}]_{10}$ superlattice. The discrete hysteresis steps are not observed at temperatures below 220 K. Within the accessible range, H_1 increases linearly with decreasing

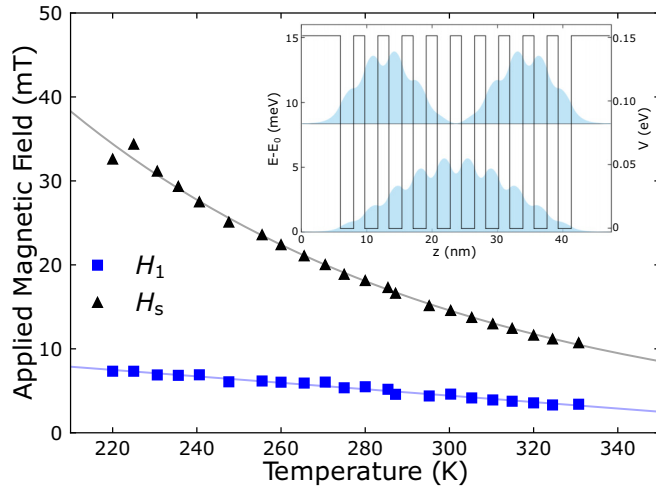


FIG. 5. Temperature dependence of the field required to switch the outermost Fe layers (H_1) in a sample with $N = 10$ and to align all layers parallel to the external field (H_s) along the easy axis ([001]). The field H_1 increases linearly with decreasing temperature and is fitted by $H_1(T) = a \cdot T + b$ ($a = -0.04$, $b = 16$), while H_s is fitted using $H_s(T) = a \cdot e^{-bT}$ ($a = 365$, $b = 0.99$). The inset shows calculated collective quantum-well state formed in a $[\text{Fe}(2.0 \text{ nm})/\text{MgO}(2.0 \text{ nm})]_{10}$ superlattice, computed using the nextnano simulation package [31]. We illustrate the ground and the first-excited state, highlighting their spatial extension across the superlattice. The spin state of the electron is ignored in these calculations.

temperature, while the saturation field increases exponentially. Consequently, the ratio of the effective coupling of the outermost and innermost layers is found to increase exponentially with decreasing temperature, reaching a value close to 5 at 220 K, as seen in Fig. 5.

The temperature dependence of the IEC, along with its sensitivity to the number of bilayer repetitions N , highlights the necessity of incorporating interactions beyond nearest neighbors when describing the magnetic properties of ferromagnet/insulator heterostructures such as Fe/MgO(001). Furthermore, if the coupling between the layers were governed by thermally activated processes such as incoherent tunneling, the coupling strength would be expected to increase [6,32] with temperature—contrary to our experimental observations. We therefore need to ask if our understanding of the interaction in these structures is incomplete. In an attempt to address that we performed calculations based on a simplified one-dimensional potential-well model, not accounting for, e.g., spin-dependent effects. The results are presented as an inset in Fig. 5. The partially delocalized states form *minibands*, with energy-level spacings on the order of a few to tens of meV [33]. In the ground state, the density of states associated with the miniband is lowest near the boundaries of the sample, due to quantum confinement and boundary-induced interference of the wave functions. This provides an intuitive rationale for the observed difference in coupling strength between the outermost and the inner layers. The temperature dependence can also be qualitatively captured by this description: as temperature increases, thermal population of

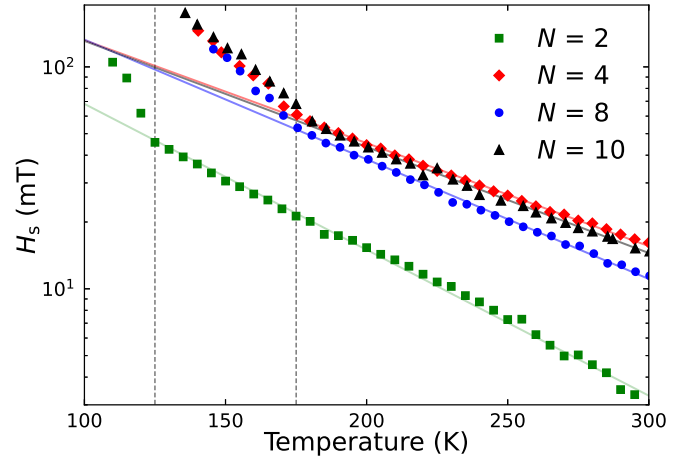


FIG. 6. Temperature dependence of the saturation field (H_s) in samples with $N = 2, 4, 8$, and 10 bilayer repetitions. Solid lines represent linear fits corresponding to an exponential increase of H_s with temperature, while dashed lines indicate the temperature below which H_s deviates from the high-temperature behavior.

higher miniband states reduces the effective overlap between wave functions in adjacent ferromagnetic layers, resulting in a weakening the interlayer exchange. Notably, this would lead to a difference in the behavior of the outermost layers in the structure with $N = 10$ as compared to the sample with only two magnetic layers. The switching field of the outermost layers have a linear temperature dependence (see Fig. 5), while the coupling strength of the interior part of the sample increases exponentially with decreasing temperature. The exchange coupling in the sample with two Fe layers, $N = 2$, is exponential, as illustrated in Fig. 6. Similar trend is observed across all samples, as seen in the figure. While the saturation field H_s remains significantly lower for $N = 2$ at elevated temperatures, it initially increases more rapidly with decreasing temperature, as compared to the other samples in the series.

III. CONCLUSIONS

Assuming the energy levels follow a particle-in-a-box model, the level spacing is expected to scale as $E_n \approx 1/N^2$, which is not observed here. Hence, a more detailed description of the interplay of the different length scales is needed to capture the oscillatory dependence on N . While these simplified analyses provide qualitative insight into the underlying mechanisms, more rigorous theoretical treatments—including spin degrees of freedom—are needed to fully quantify the contributions to the observed temperature dependence. If this interpretation is correct, our results not only advance the understanding of IEC in insulating heterostructures, but also suggest new design principles for achieving functionality in such superlattice-based devices.

ACKNOWLEDGMENTS

The authors acknowledge financial support from the Swedish Research Council (Projects No. 2021-00159 and No. 2019-03581), and support with the nextnano simulations and fruitful discussions with Dr. A. Ravensburg and

Dr. S. D. Slöetjes. Support by the Super ADAM and ILL staff is also greatly acknowledged.

DATA AVAILABILITY

The data supporting this study's findings are available within the article.

-
- [1] L. L. Chang, L. Esaki, W. E. Howard, and R. Ludeke, The growth of a GaAs–GaAlAs superlattice, *J. Vac. Sci. Technol.* **10**, 11 (1973).
- [2] A. Segmüller, P. Krishna, and L. Esaki, X-ray diffraction study of a one-dimensional GaAs–AlAs superlattice, *J. Appl. Crystallogr.* **10**, 1 (1977).
- [3] A. Gossard, GaAs/AlAs layered films, *Thin Solid Films* **57**, 3 (1979).
- [4] I. K. Schuller, New class of layered materials, *Phys. Rev. Lett.* **44**, 1597 (1980).
- [5] L. Esaki and R. Tsu, Superlattice and negative differential conductivity in semiconductors, *IBM J. Res. Dev.* **14**, 61 (1970).
- [6] P. Bruno, Theory of interlayer magnetic coupling, *Phys. Rev. B* **52**, 411 (1995).
- [7] J. Faure-Vincent, C. Tiusan, C. Bellouard, E. Popova, M. Hehn, F. Montaigne, and A. Schuhl, Interlayer magnetic coupling interactions of two ferromagnetic layers by spin polarized tunneling, *Phys. Rev. Lett.* **89**, 107206 (2002).
- [8] Y. F. Chiang, J. J. I. Wong, X. Tan, Y. Li, K. Pi, W. H. Wang, H. W. K. Tom, and R. K. Kawakami, Oxidation-induced bi-quadratic coupling in Co/Fe/MgO/Fe(001), *Phys. Rev. B* **79**, 184410 (2009).
- [9] A. Kozioł-Rachwał, T. Ślczak, M. Ślczak, K. Matlak, E. Młyńczak, N. Spiridis, and J. Korecki, Antiferromagnetic interlayer exchange coupling in epitaxial Fe/MgO/Fe trilayers with MgO barriers as thin as single monolayers, *J. Appl. Phys.* **115**, 104301 (2014).
- [10] R. Moubah, F. Magnus, T. Warnatz, G. K. Palsson, V. Kapaklis, V. Ukleev, A. Devishvili, J. Palisaitis, P. O. A. Persson, and B. Hjörvarsson, Discrete layer-by-layer magnetic switching in Fe/MgO(001) superlattices, *Phys. Rev. Appl.* **5**, 044011 (2016).
- [11] S. S. P. Parkin, C. Kaiser, A. Panchula, P. M. Rice, B. Hughes, M. Samant, and S.-H. Yang, Giant tunneling magnetoresistance at room temperature with MgO (100) tunnel barriers, *Nat. Mater.* **3**, 862 (2004).
- [12] S. Yuasa and D. D. Djayaprawira, Giant tunnel magnetoresistance in magnetic tunnel junctions with a crystalline MgO(001) barrier, *J. Phys. D* **40**, R337 (2007).
- [13] S. Bhatti, R. Sbiaa, A. Hirohata, H. Ohno, S. Fukami, and S. Piramanayagam, Spintronics based random access memory: A review, *Mater. Today* **20**, 530 (2017).
- [14] X. Lou, Z. Gao, D. V. Dimitrov, and M. X. Tang, Demonstration of multilevel cell spin transfer switching in MgO magnetic tunnel junctions, *Appl. Phys. Lett.* **93**, 242502 (2008).
- [15] S. S. P. Parkin, M. Hayashi, and L. Thomas, Magnetic domain-wall racetrack memory, *Science* **320**, 190 (2008).
- [16] F. Magnus, T. Warnatz, G. K. Palsson, A. Devishvili, V. Ukleev, J. Palisaitis, P. O. A. Persson, and B. Hjörvarsson, Sequential magnetic switching in Fe/MgO(001) superlattices, *Phys. Rev. B* **97**, 174424 (2018).
- [17] T. Warnatz, F. Magnus, N. Strandqvist, S. Sanz, H. Ali, K. Leifer, A. Vorobiev, and B. Hjörvarsson, The impact of number of repeats N on the interlayer exchange in $[\text{Fe}/\text{MgO}]_N(001)$ superlattices, *Sci. Rep.* **11**, 1942 (2021).
- [18] A. L. Ravensburg, M. P. Grassi, B. Hjörvarsson, and V. Kapaklis, Effect of iron layer thickness on the interlayer exchange coupling in Fe/MgO (001) superlattices, *Phys. Rev. B* **109**, 224404 (2024).
- [19] See Supplemental Material at <http://link.aps.org/supplemental/10.1103/r9vz-kqvm> for details of sample fabrication, additional polarized neutron reflectivity analysis, and supplementary magnetic measurements.
- [20] S. Chung, S. Lee, T. Yoo, H. Lee, J.-H. Chung, M. S. Choi, S. Lee, X. Liu, J. K. Furdyna, J.-H. Han, H.-W. Lee, and K.-J. Lee, The critical role of next-nearest-neighbor interlayer interaction in the magnetic behavior of magnetic/non-magnetic multilayers, *New J. Phys.* **15**, 123025 (2013).
- [21] H. Xu, F. Chen, B. Chen, F. Jin, C. Ma, L. Xu, Z. Guo, L. Qu, D. Lan, and W. Wu, Synthetic antiferromagnets with steplike hysteresis loops and high- T_C based on all-perovskite $\text{La}_{0.7}\text{Sr}_{0.3}\text{MnO}_3$ superlattices, *Phys. Rev. Appl.* **10**, 024035 (2018).
- [22] T. Warnatz, B. E. Skovdal, F. Magnus, H. Stopfel, D. Primetzhofer, A. Stein, R. Brucas, and B. Hjörvarsson, The influence of diameter on the magnetic saturation in $\text{Fe}_{84}\text{Cu}_{16}/\text{MgO}[001]$ multilayered islands, *J. Magn. Magn. Mater.* **496**, 165864 (2020).
- [23] A. A. Fraerman, B. A. Gribkov, S. A. Gusev, A. Y. Klimov, V. L. Mironov, D. S. Nikitushkin, V. V. Rogov, S. N. Vdovichev, B. Hjörvarsson, and H. Zabel, Magnetic force microscopy of helical states in multilayer nanomagnets, *J. Appl. Phys.* **103**, 073916 (2008).
- [24] M. van Kampen, I. L. Soroka, R. Bručas, B. Hjörvarsson, R. Wieser, K. D. Usadel, M. Hanson, O. Kazakova, J. Grabis, H. Zabel, C. Jozsa, and B. Koopmans, On the realization of artificial XY spin chains, *J. Phys.: Condens. Matter* **17**, L27 (2005).
- [25] A. Kozioł-Rachwał, W. Skowroński, M. Frankowski, J. Chęciński, S. Ziętek, P. Rzeszut, M. Ślczak, K. Matlak, T. Ślczak, T. Stobiecki, and J. Korecki, Interlayer exchange coupling, dipolar coupling and magnetoresistance in Fe/MgO/Fe trilayers with a subnanometer MgO barrier, *J. Magn. Magn. Mater.* **424**, 189 (2017).
- [26] C. Bellouard, J. Faure-Vincent, C. Tiusan, F. Montaigne, M. Hehn, V. Leiner, H. Fritzsche, and M. Gierlings, Interlayer magnetic coupling in Fe/MgO junctions characterized by vector magnetization measurements combined with polarized neutron reflectometry, *Phys. Rev. B* **78**, 134429 (2008).
- [27] A. Vorobiev, A. Devishvili, G. Palsson, H. Rundlöf, N. Johansson, A. Olsson, A. Dennison, M. Wolff, B. Giroud, O. Aguetz, and B. Hjörvarsson, Recent upgrade of the polarized

- neutron reflectometer super ADAM, *Neutron News* **26**, 25 (2015).
- [28] A. Klechikov, Pysared v1.5.1 (2021), <https://www.ill.eu/users/instruments/instruments-list/superadam/software>.
- [29] M. Björck and G. Andersson, *GenX*: An extensible X-ray reflectivity refinement program utilizing differential evolution, *J. Appl. Crystallogr.* **40**, 1174 (2007).
- [30] A. Glavic and M. Björck, *GenX 3*: The latest generation of an established tool, *J. Appl. Crystallogr.* **55**, 1063 (2022).
- [31] S. Birner, T. Zibold, T. Andlauer, T. Kubis, M. Sabathil, A. Trellakis, and P. Vogl, Nextnano: General purpose 3-D simulations, *IEEE Trans. Electron Devices* **54**, 2137 (2007).
- [32] J. C. Slonczewski, Conductance and exchange coupling of two ferromagnets separated by a tunneling barrier, *Phys. Rev. B* **39**, 6995 (1989).
- [33] *Springer Handbook of Electronic and Photonic Materials*, edited by S. Kasap and P. Capper (Springer, New York, 2006).